Electronic Supplementary Information for

A thin carbon nanofibers/branched carbon nanofibers nanocomposite

for high-performance supercapacitors

Yongsheng Zhou[a,b,c], *Shibiao Xu*[b], *Jiaojiao Yang*[b], *Ziyu Zhou*[b], *Shou Peng*[a], *Xuchun Wang*[b], *Tingting Yao*[a], *Yingchun Zhu*[c,d], *Bingshe Xu*[e], *and Xueji Zhang*[f]

[a] State Key Laboratory of Advanced Technology for Float Glass, Bengbu, 233018, P. R. China

[b] College of Chemistry and Materials Engineering, Anhui Science and Technology University, Bengbu, 233030, P. R. China

[c] Key Laboratory of Inorganic Coating Materials CAS, Shanghai Institute of Ceramics, Chinese Academy of Sciences, Shanghai, 200050, P. R. China

[d] Center of Materials Science and Optoelectronics Engineering，University of Chinese Academy of Sciences, Beijing 100049, P. R. China

[e] Key Laboratory of Interface Science and Engineering in Advanced Materials, Ministry of Education, Taiyuan University of Technology, Taiyuan, 030024, P. R. China

[f] School of Biomedical Engineering, Shenzhen University Health Science Center, Shenzhen, Guangdong 518060, P. R. China

E-mail: yszhou1981@gmail.com; E-mail: zhangxueji@szu.edu.cn

Experimental section

Synthesis of N-doped thin carbon nanofibers hang on branched carbon nanofibers (TCNF/CNF)

0.5 g of polyacrylonitrile (PAN) and 0.25 g of polyvinylpyrrolidone (PVP) were dissolved in 4.25 g of dimethylformamide (DMF) at room temperature under magnetic stirring to form a polymer solution after stirring for 3 h to ensure complete solubility. A 4.0 g amount of $Ni(Ac)_2$ (Ac = acetate) and magnesium nitrate hexahydrate was added to the mixture, and stirring was continued until the polymer solution became clear and then loaded into a 5 mL plastic syringe. The electrospinning process was carried out at a high voltage of 20 kV at a feeding rate of 0.1 mm min^{-1} through a stainless-steel needle, which had an inner diameter of 0.5 mm. After evaporation of the solvents from the jet stream, the composite nanofibers of $PAN/PVP/Ni(Ac)_2/Mg(NO_3)_2$ were produced and the resulting nonwoven fiber mat was collected. All electrospinning experiments were performed at room temperature. The obtained nonwoven fiber mat was stabilized in air at 265 °C for 3 h with a heating rate of 1 °C/min.

Then, the preoxidized process of the generated $PAN/PVP/Ni(Ac)_2/Mg(NO_3)_2$ nanofiber membrane was generated at 180 °C in air atmosphere for 1 h with a heating rate of 1 °C min^{-1}. TCNF/CNF was grown on the resulting product at 850 °C under a gas mixture (C_2H_2: Ar: NH_3=100: 500: 100 sccm) flow in an induction furnace. The TCNF-N was harvested after the acidic etching of the sample by a HCl solution to remove MgO. The CNF material was prepared in a way similar to that for the TCNF/CNF material, but PVP was not added to the reaction.

Characterization of materials

The morphology of the cross section of the nanofibrils-based films was studied by scanning electron microscopy (SEM) (SU-7000 SEM, Hitachi, Japan). The transmission electron microscope (TEM) images were obtained using a FEI Titan G_2 60-300 operating at 80 kV. Raman spectra were recorded with a Renishaw RM-1000 Micro Raman Spectrometer. Investigations of chemical compositions were performed using X-ray photoelectron spectroscopy (XPS, Physical Electronics PHI 5600). N_2 sorption analysis was conducted on an ASAP2020 accelerated surface area and porosimetry instrument (Micromeritics), equipped with automated surface area, at 77 K using BarrettEmmettTeller (BET) calculations for the surface area. The pore size distribution (PSD) plot was recorded from the adsorption branch of the isotherm based on the Barrett−Joyner−Halenda (BJH) method.

Electrochemical measurements

5 mg of the activated TCNF/CNF, CNF materials were pressed into electrode films using a standard preforming mold with a pressure of 5 t. Electrochemical experiments were performed in several configurations and electrolytes. For aqueous electrolyte, 1.0 M H_2SO_4 (pH 0) solution was used. In three-electrode cells, in addition to the working electrode of active material, platinum as the counter electrode and Ag/AgCl as the reference electrode were used. In symmetric cells, two identical (by weight, size and composition) active-material electrodes were used as cathode and anode. Cyclic voltammetry (CV) tests and galvanostatic charge–discharge (GCD) tests were performed using an electrochemical analyzer, CHI 660E, under ambient conditions. Electric impedance spectroscopy (EIS) was performed with an amplitude of 10 mV, from 10 mHz to 100 kHz.

Symmetric devices with two identically configured electrodes were also packaged. Since the electrodes were highly conductive, they were directly connected to the electrochemical analyzer by alligators without any current collector. After inserting an ion-porous separator (Celgard 3501) between the two electrodes, the electrode/electrolyte assembly was wrapped within a Kapton tape seal to complete the package.

The specific capacitance (C for CV curves and Cs for GCD curves, Cs1 for three-electrode and Cs2 for two-electrode configuration), the energy density (E) and the power density (P) of these cells were calculated using the following equations:

a. the calculation of specific capacitance by GCD curves in three-electrode configuration:

$$C_{s1} = \frac{I}{m \cdot (dV/dt)}$$
(1)

b. the calculation of specific capacitance by GCD curves in two-electrode configuration:

$$C_{s2} = \frac{4I}{m \cdot (dV/dt)}$$
(2)

Where I (A) is the discharge current, S (V s^{-1}) is the scan rate, dV/dt is the slope of the discharge curve (V s^{-1}), m (g) is the mass of the single working electrode, and ΔV (V) denotes the voltage change excluding the IR drop during the discharge process.

c. the calculation of energy density (E) and power density (P):

$$E = \frac{C_S \cdot \Delta V^2}{2 \cdot 3.6}$$
(3)

$$P = \frac{E \cdot 3600}{\Delta t}$$
(4)

Where ΔV (V) denotes the voltage change excluding the IR drop during the discharge process, and

Δt (s) is the discharge time.
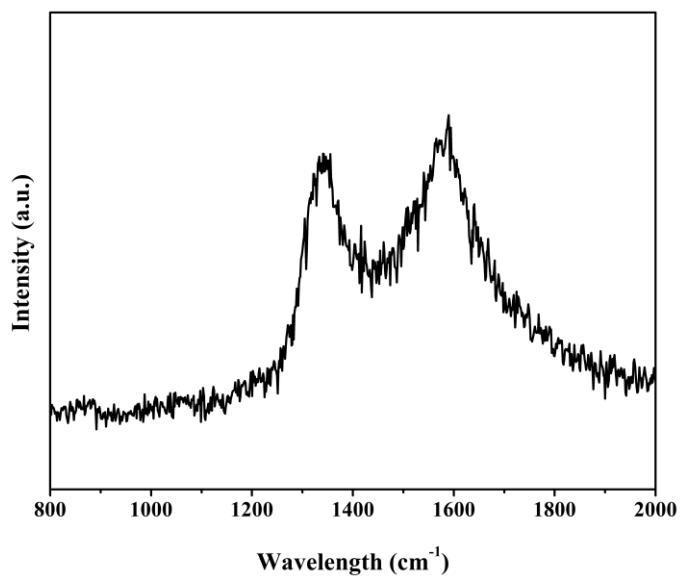
Figure S1. Raman spectra of TCNF/CNF.
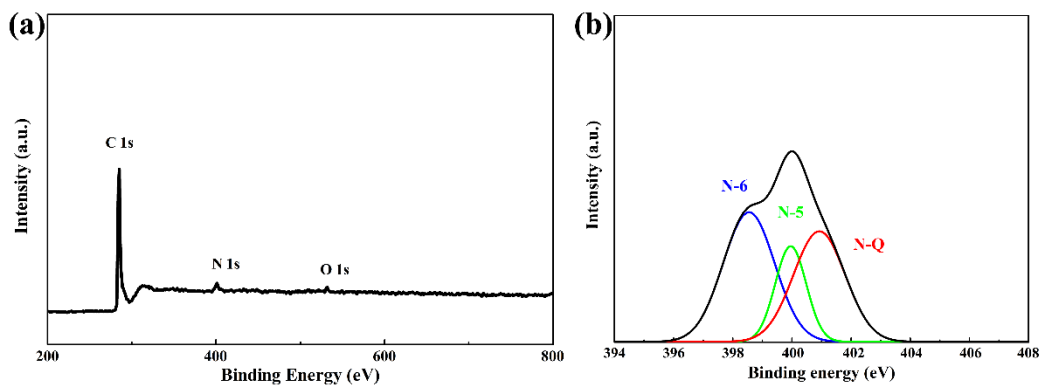
Figure S2. (a) XPS survey, and (b) the fine-scanned N 1s spectra of TCNF/CNF.
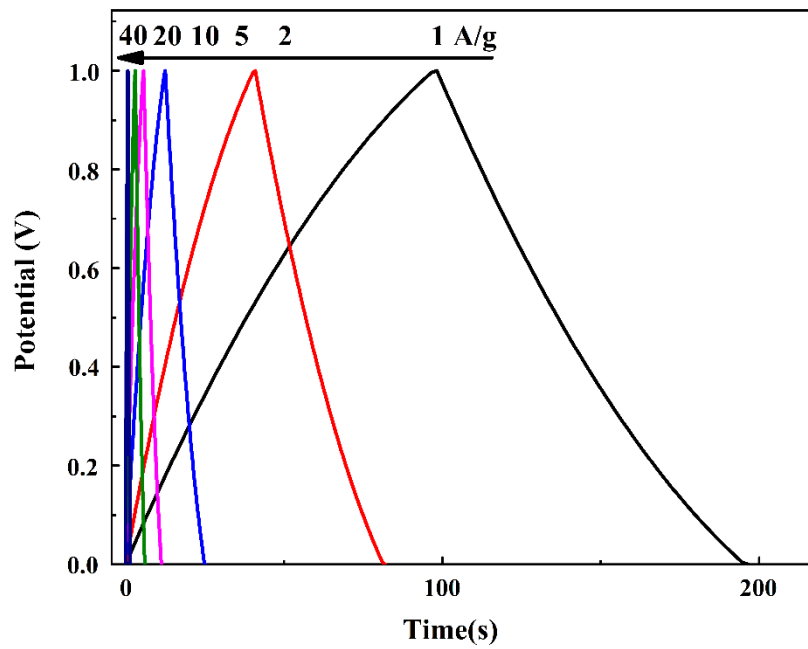
Figure S3. GCD curves of CNF at the current densities.
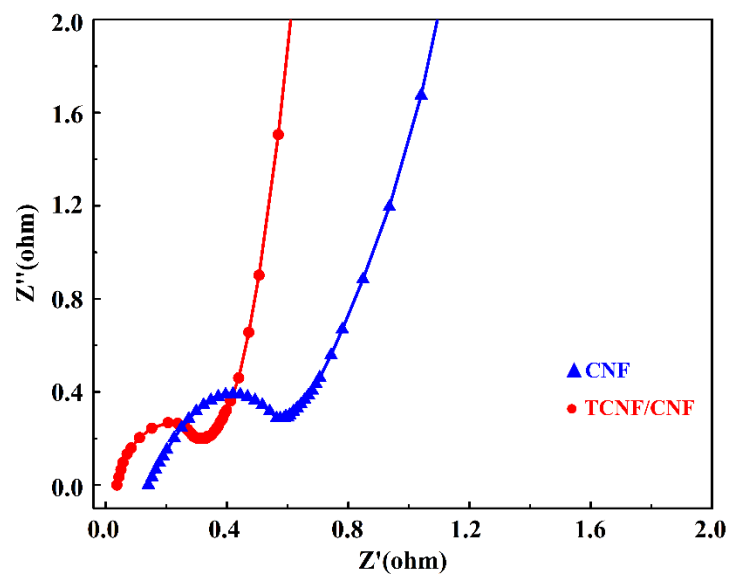
Figure S4. Typical Nyquist plot of the TCNF/CNF and CNF.

Table S1 Selected N-doped carbon-based structure for SCs.

Materials	N level (at %)	Electrolyte	Capacitance (F g^{-1}), Test configuration (2 or 3- electrode)	E (Wh kg^{-1}) /P (W kg^{-1})	Ref.
NPO-HCSs	1.33	KOH	253 at 0.2 A g^{-1}, 3	17.6/800	1
Porous NG/CNTs	4.12	KOH	247 at 0.5 A g^{-1}, 3	N/A	2
F-RGO-60	N/A	KOH	68 at 0.2 A g^{-1}, 2 217.3 at 1 A g^{-1}, 3	N/A	3
Porous N-rich carbon composite	2.3	KOH	240 at 0.1 A g^{-1}, 3	7.07/22.5	4
N-rGO/MWCNTs/NF	N/A	KOH	142 at 1 A g^{-1}, 2	N/A	5
Crumpled NG nanosheets	9.96	KOH	245.9 at 5 mV s^{-1}, 3	N/A	6
N-CNF /rGO/bacterial cellulose	4.82	KOH H$_2$SO$_4$	263 at 0.125 A g^{-1}, 3 318 at 0.125 A g^{-1}, 3	N/A	7
Ice-templated NG	6.2	KOH	217 at 5 mV s^{-1}, 3	N/A	8
NG hydrogel	9.64	KOH	190.1 at 10 A g^{-1}, 2	23.8/9000	9
NB-GA	N/A	NaOH	483 at 1 A g^{-1}, 2	22.1/8100	10
porous mycelium-derived activated carbon	N/A	H$_2$SO$_4$	190 at 1 A g^{-1}, 2	N/A	11
porous few-layer carbon	1.52	H$_2$SO$_4$	340 at 0.5 A g^{-1}, 3	8.33/6000	12
carbon aerogels	N/A	KOH	199 at 1 A g^{-1}, 3	N/A	13
Our work	9.3	H$_2$SO$_4$	224 at 1 A g^{-1}, 3	6.8/18450	

References

1. M. Gao, J. Fu, M. Wang, K. Wang, S. Wang, Z. Wang, Z. Chen, Q. Xu, *J Colloid Interface Sci.* **2018**, 6;524:165-176.

2. T. T. Lin, W. H. Lai, Q. F. Lu, Y. Yu, *Electrochem. Acta* **2015**, 178, 517.

3. C. Huang, A. Hu, Y. Li, H. Zhou, Y. Xu, Y. Zhang, S. Zhou, Q. Tang, C. Chen, X. Chen, *Nanoscale* **2019**,11(35):16515-16522.

4. X. M. Fan, C. Yu, J. Yang, Z. Ling, J. S. Qiu, *Carbon* **2014**, 70, 130.

5. F. Y. Bana, S. Jayabala, H. N. Limb, H. W. Leec, N. M. Huang, *Ceram. Int*. **2017**, 43, 20.

6. Z. Wen, X. Wang, S. Mao, Z. Bo, H. Kim, S. Cui, G. Lu, X. Feng, J. Chen, *Adv. Mater*. **2012**, 24, 5610.

7. J. Yang, E. Zhang, X. Li, Y. Yu, J. Qu, Z. Z. Yu, *ACS Appl. Mater. Inter*. **2016**, 8, 2297.

8. M. Kota, X. Yu, S. Yeon, H. Cheong, H. S. Park, *J. Power Sources* **2016**, 303, 372.

9. P. Chen, J. J. Yang, S. S. Li, Z. Wang, T. Y. Xiao, Y. H. Qian, S. T. Yu, *Nano Energy* **2013**, 2, 249.

10. Y. Shabangoli, M. S. Rahmanifar, A. Noori, M. F. El-Kady, R. B. Kaner, M. F. Mousavi. *ACS Nano* **2019**, doi: 10.1021/acsnano.9b03351.

11. J. Hao, Y. Huang, C. He, W. Xu, L. Yuan, D. Shu, X. Song, T. Meng. *Sci Rep*. **2018**, 8(1):562

12. M. Qian, Y. Wang, F. Xu, W. Zhao, T. Lin, F. Huang. *ACS Appl Mater Interfaces*. **2018**,10(1):381-388.

13. M. Zhang, M. Chen, N. Reddeppa, D. Xu, Q. Jing, R. Zha, *Nanoscale*. **2018**, 5;10(14):6549-6557.